Research Square

Preprints are preliminary reports that have not undergone peer review.
They should not be considered conclusive, used to inform clinical practice,
or referenced by the media as validated information.

Methane dynamics in wetland ecosystems: mathematical model, properties of the initial–boundary value problem and verification of the numerical scheme

Sergey P. Semenov

ssp@ugrasu.ru

Yugra State University

Artem O. Tashkin

Yugra State University

Research Article

Keywords: Methane, Peatland, Ebullition, Initial–boundary value problem, Weak solution, Finite volume method

Posted Date: November 13th, 2026

DOI: https://doi.org/10.21203/rs.3.rs-11564865/v1

License: This work is licensed under a Creative Commons Attribution 4.0 International License.
Read Full License

Additional Declarations: No competing interests reported.

Methane dynamics in wetland ecosystems: mathematical model, properties of the initial–boundary value problem and verification of the numerical scheme

Sergey P. Semenov[1*] · Artem O. Tashkin[1]

[1]Yugra State University, 16 Chekhova St., Khanty-Mansiysk, 628012, Russia
*Corresponding author: ssp@ugrasu.ru; contributing author: anozer_sky@mail.ru

Abstract A one-dimensional vertical model of dissolved methane dynamics in water-saturated peat is formulated and analysed. The model accounts for methanogenesis, Monod-type oxidation, molecular diffusion, ebullition with a threshold determined by the atmospheric, hydrostatic and capillary pressures, and plant-mediated transport represented by a point sink at the root uptake level; mass exchange with the atmosphere is imposed on the total flux at the surface by a Robin condition. For the problem with a truncated bubble flux, a weak formulation is introduced, and the existence, uniqueness and non-negativity of the weak solution and its continuous dependence on the initial data and the source are proved. The point sink is shown to be well defined without regularization and to be equivalent to an interface condition with a jump of the diffusive flux. For the stationary problem, the existence of a non-negative solution is established, together with its uniqueness and exponential stability under a smallness condition, and a sufficient condition for a zero bubble flux through the surface is obtained. A conservative monotone finite-volume scheme with exponential fitting of the fluxes, upwind evaluation of the bubble velocity and the implicit Euler method is constructed. Its MATLAB implementation is verified against two analytical steady-state solutions and by the method of manufactured solutions: the scheme conserves mass to machine precision and exhibits second-order spatial convergence without active ebullition and first-order convergence with active bubble transport and in time.

Keywords Methane · Peatland · Ebullition · Initial–boundary value problem · Weak solution · Finite volume method

MSC Classification 35K20, 35K59, 35D30, 65M08, 65M12, 92D40

1 Introduction

Natural wetlands are the largest natural source of methane and one of the most uncertain components of its global budget [1]. In peat, methane is produced in the anaerobic zone, is partly oxidized in the near-surface layer and in the rhizosphere, and is transported to the atmosphere by diffusion, ebullition, and through the aerenchyma of plants [2–4]. The considerable heterogeneity of methane emission from West Siberian mires [5–9] calls for an explicit account of the mechanisms that form it.

Methane dynamics in wetland ecosystems has been modelled at many levels of detail, from one-dimensional profile models to modules of global vegetation and climate models. Among them, the closest to the present formulation in terms of the processes described is the model of Walter and Heimann [10], which has also been applied to West Siberian mires [11]. It describes the profile of dissolved CH_4 taking into account production, oxidation, diffusion, bubble and plant-mediated transport. Ebullition is specified as a sink activated when a fixed threshold is exceeded, plant uptake is distributed over the root layer, and a prescribed concentration (Dirichlet

condition) is imposed at the surface. The model is therefore a convenient point of comparison, although its boundary conditions and the form of bubble transport differ from those adopted here.

In the LPJ-WHyMe and CLM4Me models the ebullition threshold is related to the local pressure [12, 13]; more detailed modules have been developed in JSBACH-methane [14] and HIMMELI [15]. A capillary correction to the threshold has been used for lake sediments [16], and an effective advective transport in ISBA [17]. A comparison of ebullition schemes shows that the temporal structure of the emission and its partitioning among the pathways depend on the way ebullition is described [18]. The WETCHIMP-WSL model intercomparison revealed a considerable spread of the emission estimates for West Siberia [19]. Thus, the mechanisms themselves and their parameterizations have already been described in the literature, but their combination and consistency within a single mathematical formulation remain a subject of research.

In the present paper, the ebullition threshold depends on the local pressure and temperature, and bubble transport arises when the concentration of dissolved methane exceeds this threshold. Bubble transport is described as an effective upward flux inside the peat column, plant uptake is specified by a point sink at the root uptake level, and a condition of mass exchange with the atmosphere is imposed at the surface on the total (diffusive and bubble) flux, while plant-mediated transport bypasses the surface through the point sink. This combination is a chosen mathematical idealization rather than a new physical theory of bubble formation.

The aim of this paper is to formulate an initial–boundary value problem for the dynamics of dissolved methane in water-saturated peat, to study its well-posedness, and to construct a verified algorithm for its numerical solution in MATLAB. The paper continues our earlier studies [20–22]. The known well-posedness results for simpler problems of methane uptake [23, 24] do not cover the threshold nonlinearity of bubble transport or the point sink; therefore, the present formulation requires a separate analysis.

The main results of the paper are as follows.

- A one-dimensional model is derived from the mass conservation law for an arbitrary peat layer (Sects. 2, 3). In the model, methanogenesis and Monod-type oxidation depend on temperature. The ebullition threshold is determined by the atmospheric, hydrostatic and capillary pressures; bubble transport is described by an effective upward flux, and plant-mediated transport by a δ-sink at the root uptake level. A Robin condition is imposed on the total flux at the surface.
- For the problem with a truncated bubble flux, a weak solution is introduced. Its existence, uniqueness and non-negativity are proved, and an energy estimate and an estimate of continuous dependence on the initial data and the source are obtained (Theorems 1 and 2). The δ-sink is shown to be well defined without regularization and to generate, at the root uptake level, an interface condition with a jump of the diffusive flux (Theorem 3). The weak solution satisfies the integral mass balance (Corollary 1).
- For the stationary problem, the existence of a non-negative solution is proved. If the Lipschitz constant of the bubble flux is small, this solution is unique and exponentially stable (Theorem 4). A sufficient condition is found under which the stationary bubble flux through the surface vanishes (Theorem 5).
- A conservative monotone finite-volume scheme is constructed. It uses exponential fitting of the fluxes, upwind evaluation of the bubble velocity and the implicit Euler method. The scheme reproduces the discrete mass balance exactly and preserves the non-negativity of the solution (Sect. 5).

- Analytical steady-state solutions of two test problems are obtained: with a δ-sink and a Robin condition (problem A) and with a thin internal layer (problem B) (Sect. 4).
- The numerical scheme is verified against the two analytical solutions and by the method of manufactured solutions; these tests confirm second-order spatial convergence without ebullition and first-order convergence with active ebullition and in time, and the mass balance holds to machine precision (Sects. 6, 7).

The paper is organized as follows. Section 2 describes the conceptual scheme, and Sect. 3 derives the initial–boundary value problem and studies its properties (Sect. 3.7). Section 4 contains analytical solutions of the test problems, Sect. 5 the numerical scheme, and Sects. 6 and 7 the comparison with the analytical solutions and the convergence study; conclusions are stated in Sect. 8.

2 Conceptual scheme of methane dynamics

2.1 Domain and main variables

We consider a vertical column of water-saturated peat $0 \le z \le L$ on the time interval $0 \le t \le t_\mathrm{f}$ (Fig. 1); the z axis points upward, and $z = L$ is the soil surface, which coincides with the water table or is covered by a water layer $H_\mathrm{w} \ge 0$. The unknown is the concentration of dissolved methane $C(t, z)$, mol m^{-3}, in the pore water; the porosity $\phi \approx 0.9$ is assumed constant. A separate gas phase, the heterogeneity of the pore space and the transport through plant tissues are not resolved: their effect is represented by averaged parameters. The water table is fixed in the computations; therefore, its fluctuations are not described by the model.

2.2 Methane production

Methanogenesis is represented by a source in the anaerobic zone whose intensity decreases with depth and depends on temperature, following [2, 10, 25]:

$$S(t,z) = \begin{cases} S_\mathrm{ref}\, e^{-(z_\mathrm{ox}-z)/\ell_S}\, Q_{10,S}^{(T(t,z)-T_\mathrm{ref})/10}\, \eta(T), & 0 \le z < z_\mathrm{ox}, \\ 0, & z_\mathrm{ox} \le z \le L. \end{cases} \tag{1}$$

Here ℓ_S is the vertical production scale, $Q_{10,S}$ is the temperature coefficient [25], and $\eta(T) = \min\{\max\{T/\Delta T_\mathrm{f}, 0\}, 1\}$ is the activity function near 0 °C; the factor S_ref is determined from the depth-integrated production $P = \int_0^L S\, dz$.

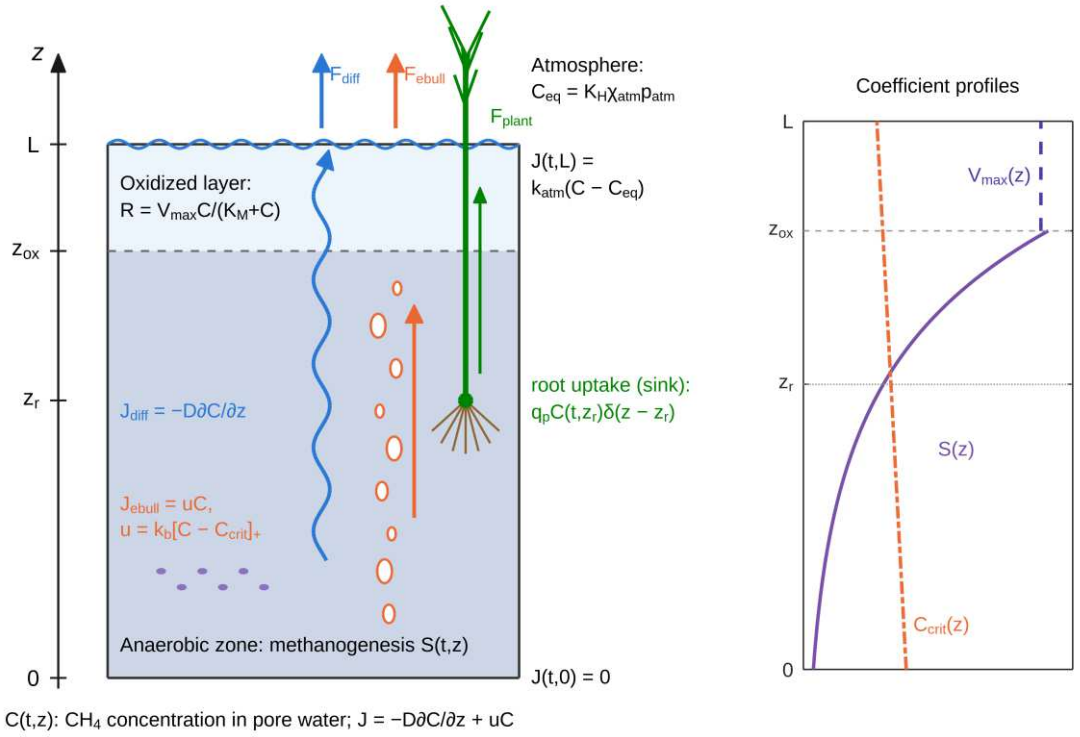


Fig. 1 Conceptual scheme of the one-dimensional model (not to scale). Left: vertical profile of the peat deposit with the anaerobic zone $0 \le z < z_{\mathrm{ox}}$, the oxidized layer $z_{\mathrm{ox}} \le z \le L$, the root uptake level z_{r}, transport pathways and boundary conditions. Right: profiles of $S(z)$, $V_{\max}(z)$ and $C_{\mathrm{crit}}(z)$. The arrow F_{ebull} shows the bubble flux in the general case; conditions for a zero stationary flux through the surface are given by Theorem 5 (Sect. 3.7.8)

2.3 Methane oxidation

Methane oxidation in the near-surface zone of thickness $\delta_{\mathrm{ox}} = L - z_{\mathrm{ox}}$ is described by Monod kinetics [10, 13]. The limited penetration depth of oxygen into peat is supported by observations [26]:

$$R(t,z,C) = V_{\max}(t,z)\,\frac{C}{K_M + C},$$
$$V_{\max}(t,z) = V_{\max,\mathrm{ref}}\, Q_{10,O}^{(T-T_{\mathrm{ref}})/10}\,\eta(T)\,\mathbf{1}_{\{z \ge z_{\mathrm{ox}}\}}. \tag{2}$$

The kinetic parameters, namely the maximum oxidation rate and the half-saturation constant, are taken from [10, 13] (Table 1). For $C \ll K_M$ the kinetics can be linearized:

$$R \approx k\,C, \qquad k = \frac{V_{\max}}{K_M}, \qquad C \ll K_M. \tag{3}$$

At the concentrations typical of peat, $C/K_M \sim 10^2$, the linear approximation may overestimate oxidation [26]; therefore, Monod kinetics is used in the full model, and the linearization only in the test problems (Sect. 4).

2.4 Diffusive transport

$$J_{\mathrm{diff}} = -D\,\frac{\partial C}{\partial z}, \qquad D = \xi\, D_{\mathrm{w}}(T),$$
$$D_{\mathrm{w}}(T) = (0.9798 + 0.02986\,T + 0.0004381\,T^2)\cdot 10^{-9}\ \mathrm{m^2\,s^{-1}}. \tag{4}$$

Methane diffusion is described by Fick's law (4), where D_{w} is the diffusion coefficient of CH_4 in water [12, 13] (T in °C) and $\xi = 0.66$ is the tortuosity correction for the pore space [10]. In the computations $D \approx 1.0 \cdot 10^{-9}$ m² s⁻¹ (with ξ from Table 1 and $T = T_{\mathrm{ref}}$).

2.5 Ebullition

The solubility of methane is described by Henry's law [27]:

$$C = K_H(T)\, p_{\mathrm{CH_4}}, \qquad K_H(T) = K_H^{\circ} \exp\left[\Theta\left(\frac{1}{T + 273.15} - \frac{1}{298.15}\right)\right]. \tag{5}$$

Bubbles are not modelled as a separate gas phase. They are assumed to form when the concentration of dissolved methane exceeds the value in equilibrium with the bubble gas. The partial pressure of methane in a bubble is $p_{\mathrm{CH_4}} = x_{\mathrm{b}}\, p_{\mathrm{loc}}$, where x_{b} is the mole fraction of methane in the bubble gas and p_{loc} is the local pressure. The latter is the sum of the atmospheric, hydrostatic and capillary components; the capillary component is determined by the surface tension σ and the pore radius r [16]. The ebullition threshold is then

$$C_{\mathrm{crit}}(t, z) = K_H(T)\, x_{\mathrm{b}} \left[p_{\mathrm{atm}} + \rho_{\mathrm{w}} g\, (L - z + H_{\mathrm{w}}) + \frac{2\sigma}{r}\right]. \tag{6}$$

The effect of bubbles on methane transport is represented by an upward flux that arises when the concentration exceeds the threshold:

$$J_{\mathrm{ebull}} = u(t, z, C)\, C, \qquad u = k_{\mathrm{b}} \max\{C - C_{\mathrm{crit}}(t, z), 0\}. \tag{7}$$

The coefficient k_{b} sets the intensity of this transport.

In contrast to the constant threshold of the Walter–Heimann model [10], threshold (6) depends on the local pressure and temperature. The capillary correction has previously been applied to lake sediments [16] and is therefore not new by itself. The effect of atmospheric pressure on ebullition has been shown in [28, 29], and the features of bubble release from peat are described in [30, 31].

2.6 Plant-mediated transport

Plants with aerenchyma take up methane from the root zone and transport it to the atmosphere, bypassing the oxidized layer [4]. This is described by a point sink at the root level $z_{\mathrm{r}} < z_{\mathrm{ox}}$:

$$S_{\mathrm{plant}}(t, z) = q_{\mathrm{p}}\, C(t, z_{\mathrm{r}})\, \delta(z - z_{\mathrm{r}}), \qquad q_{\mathrm{p}} = f_{\mathrm{cover}}\, K_{\mathrm{plant}}. \tag{8}$$

In (8), f_{cover} is the fraction of the area covered by aerenchymatous plants, K_{plant} is the conductance of the plant pathway with rhizospheric oxidation taken into account, and δ is the Dirac delta function localizing the uptake at the level z_{r} [4, 10, 12].

The emission is the sum of the diffusive, bubble and plant-mediated fluxes: $F_{\mathrm{total}} = F_{\mathrm{diff}} + F_{\mathrm{ebull}} + F_{\mathrm{plant}}$, where $F_{\mathrm{plant}} = q_{\mathrm{p}} C(t, z_{\mathrm{r}})$.

3 Mathematical model of methane dynamics

3.1 Derivation of the mass balance equation

The mass conservation law for an arbitrary layer $[z_1, z_2] \subset (0, L)$ with the total flux $J = -D\ \partial_z C + uC$ reads

$$\frac{d}{dt}\int_{z_1}^{z_2} C\ dz = J(t,z_1) - J(t,z_2) + \int_{z_1}^{z_2}(S-R)\ dz - q_{\mathrm{p}}\,C(t,z_{\mathrm{r}})\,\mathbf{1}_{\{z_1<z_{\mathrm{r}}<z_2\}}. \tag{9}$$

For a sufficiently smooth solution, this yields the convection–diffusion–reaction equation

$$\frac{\partial C}{\partial t} = \frac{\partial}{\partial z}\left(D\,\frac{\partial C}{\partial z}\right) - \frac{\partial (uC)}{\partial z} + S(t,z) - R(t,z,C) - q_{\mathrm{p}}\,C(t,z_{\mathrm{r}})\,\delta(z-z_{\mathrm{r}}). \tag{10}$$

The integral form (9) remains valid where the solution is not differentiable (at the point z_{r}); it underlies the weak formulation and the finite-volume method.

3.2 Initial condition

$C(0,z) = C_0(z) \geq 0,\ 0 \leq z \leq L.$

3.3 Bottom boundary condition

No methane enters through the bottom boundary; therefore, the total flux vanishes there:

$$J(t,0) = -D\,\frac{\partial C}{\partial z}(t,0) + u(t,0)\,C(t,0) = 0. \tag{11}$$

Condition (11) means that the bottom boundary is impermeable to the combined diffusive and bubble flux.

3.4 Top boundary condition and closure of the problem

Mass exchange with the atmosphere is imposed at the surface for the total diffusive and bubble flux (a Robin-type boundary condition):

$$-D\,\frac{\partial C}{\partial z}(t,L) + u(t,L)\,C(t,L) = k_{\mathrm{atm}}\big(C(t,L) - C_{\mathrm{eq}}\big). \tag{12}$$

In (12), $C_{\mathrm{eq}} = K_H \chi_{\mathrm{atm}} p_{\mathrm{atm}} \approx 3.2 \cdot 10^{-6}\ \mathrm{mol\,m^{-3}}$ is the concentration in equilibrium with the atmosphere according to Henry's law [1, 27]. The mass exchange coefficient is estimated by a parameterization of the gas transfer velocity from the literature [32, 33]:

$$k_{\mathrm{atm}} = k_{600}\left(\frac{Sc}{600}\right)^{-1/2}, \qquad Sc(T) = 1897.8 - 114.28\,T + 3.2902\,T^2 - 0.039061\,T^3. \tag{13}$$

where Sc is the Schmidt number of CH_4 in water (T in °C) and k_{600} is the gas transfer velocity normalized to $Sc = 600$. The value of the mass exchange coefficient adopted in Table 1 is taken from the literature and is not a measurement for the mire under study. The flux through the surface is given by condition (12), while the total emission also includes the transport through plants (8).

3.5 The initial–boundary value problem

Find $C(t,z)$ satisfying the equation

$$\begin{aligned}\frac{\partial C}{\partial t} = \frac{\partial}{\partial z}\left(D\,\frac{\partial C}{\partial z}\right) - \frac{\partial}{\partial z}\left(k_{\mathrm{b}}\max\{C - C_{\mathrm{crit}}(t,z), 0\}\,C\right) \\ + S(t,z) - \frac{V_{\max}\,C}{K_M + C} - q_{\mathrm{p}}\,C(t,z_{\mathrm{r}})\,\delta(z-z_{\mathrm{r}})\end{aligned} \tag{14}$$

with the initial condition $C(0,z) = C_0(z)$ and the boundary conditions (11), (12); the parameters are listed in Table 1.

3.6 Integral mass balance

Integration of Eq. (10) over the column height gives the mass balance used to monitor the computations:

$$\frac{dM}{dt} = P(t) - O(t) - F_{\mathrm{atm}}(t) - F_{\mathrm{plant}}(t),$$
$$M = \int_0^L C\ dz, \qquad P = \int_0^L S\ dz, \qquad O = \int_0^L R\ dz. \tag{15}$$

Here M is the column storage of dissolved methane and O is the depth-integrated oxidation rate. For the base parameters, diffusive transport from deep horizons is slower than the characteristic accumulation of methane; therefore, additional transport mechanisms have to be taken into account.

Table 1 Base values of the model parameters ($T_{\mathrm{ref}} = 15$ °C)

Symbol	Meaning	Value	Unit	Source
L	peat thickness	1.0	m	assumed
δ_{ox}	thickness of the oxidized layer	0.03	m	[26]
$L - z_{\mathrm{r}}$	rooting depth	0.20	m	assumed
H_{w}	water layer above the surface	0	m	assumed
P	production at T_{ref}	$1.0 \cdot 10^{-7}$	mol m^{-2} s^{-1}	assumed
ℓ_S	decay scale of production	0.30	m	assumed
$Q_{10,S}$	temperature coefficient of methanogenesis	2.5	–	[10, 25]
$Q_{10,O}$	temperature coefficient of oxidation	2.0	–	[10, 25]
ΔT_{f}	activity onset interval	1	°C	[10, 25]
$V_{\mathrm{max,ref}}$	maximum oxidation rate	$5.56 \cdot 10^{-6}$	mol m^{-3} s^{-1}	[10, 13]
K_M	half-saturation constant	$5 \cdot 10^{-3}$	mol m^{-3}	[10, 13]
ξ	tortuosity coefficient	0.66	–	[10]
q_{p}	conductance of the plant pathway	$3 \cdot 10^{-7}$	m s^{-1}	assumed
k_{b}	bubble conductance	10^{-5}	m^4 mol^{-1} s^{-1}	assumed
x_{b}	mole fraction of CH_4 in bubbles	0.57	–	[28]
r	pore radius	10^{-4}	m	assumed

K_H°	Henry constant at 25 °C	$1.4 \cdot 10^{-5}$	mol m^{-3} Pa^{-1}	[27]
Θ	temperature dependence parameter	1600	K	[27]
k_{atm}	mass exchange coefficient	$6.4 \cdot 10^{-6}$	m s^{-1}	[32]
χ_{atm}	mole fraction of CH_4 in the atmosphere	$1.9 \cdot 10^{-6}$	–	[1]
p_{atm}	atmospheric pressure	101 325	Pa	reference value
ρ_{w}	water density	999	kg m^{-3}	reference value
g	gravitational acceleration	9.81	m s^{-2}	reference value
σ	surface tension	0.0735	N m^{-1}	reference value

3.7 Properties of the initial–boundary value problem

3.7.1 Notation and type of the equation

We introduce the notation $\Omega = (0, L)$, $Q = (0, t_{\mathrm{f}}) \times \Omega$; $\|\cdot\|$ and $(\cdot,\cdot)$ are the norm and the inner product in $L^2(\Omega)$; $V = H^1(\Omega)$ with the norm $\| v \|_V^2 = \| v \|^2 + \| \partial_z v \|^2$, V' is its dual space, and $\langle\cdot,\cdot\rangle$ is the duality pairing between V' and V; $v^+ = \max\{v, 0\}$, $v^- = \min\{v, 0\}$. The principal part of Eq. (10) is the diffusion operator $\partial_z(D\ \partial_z C)$; hence, for $D \geq D_{\min} > 0$, the equation is a uniformly parabolic quasilinear convection–diffusion–reaction equation. Its nonlinearity is due to Monod kinetics and to the threshold dependence of the bubble velocity on the concentration, while the plant sink makes the problem nonlocal: its intensity is determined by the value of the solution at the point z_{r}. The point terms are well defined because the problem is one-dimensional: every function $v \in V$ is continuous on $[0, L]$, and its point values are bounded in terms of the norm of V (Lemma 2).

3.7.2 Truncation of the nonlinearities and assumptions

The bubble flux $f(t, z, C) = k_{\mathrm{b}} \max\{C - C_{\mathrm{crit}}, 0\}\, C$ grows quadratically for large C. For the analysis, it is replaced by the truncated flux

$$f_M(t, z, C) = k_{\mathrm{b}} \big(\Pi_M C - C_{\mathrm{crit}}(t, z)\big)^+ \Pi_M C, \qquad \Pi_M C = \min\{C^+, M\}, \tag{16}$$

where the constant $M > \sup_Q C_{\mathrm{crit}}$ is an upper bound of the physically relevant range of concentrations (in the computations of this paper the truncation is inactive: for $k_{\mathrm{b}} = 0$ the flux $f \equiv 0$, and in the test of Sect. 7.3 the solution is bounded by a known constant). Monod kinetics is extended to negative concentrations by the formula $R(t, z, C) = V_{\max}(t, z)\, C/(K_M + C^+)$. In what follows, we assume:

(A1) D, $V_{\max}$, C_{crit} are measurable bounded functions on Q, with $0 < D_{\min} \leq D \leq D_{\max}$, $0 \leq V_{\max} \leq \bar{V}$, $C_{\mathrm{crit}} \geq 0$.

(A2) $S \in L^2(Q)$, $S \geq 0$; $C_0 \in L^2(\Omega)$, $C_0 \geq 0$.

(A3) $k_{\mathrm{b}} \geq 0$, $K_M > 0$, $q_{\mathrm{p}} \geq 0$, $k_{\mathrm{atm}} > 0$, $C_{\mathrm{eq}} \geq 0$ are constants; $z_{\mathrm{r}} \in (0, L)$.

For the base parameters (Table 1) and a bounded temperature, assumptions (A1)–(A3) are satisfied.

Lemma 1 (Properties of the nonlinearities). *Let (A1) and (A3) hold. Then:*

(a) $0 \le f_M \le F_M = k_\mathrm{b} M^2$*;* $f_M(t,z,C) = 0$ *for* $C \le C_\mathrm{crit}(t,z)$*, in particular for* $C \le 0$*;* $f_M = f$ *for* $0 \le C \le M$*; the function* f_M *is non-decreasing in* C *and satisfies the Lipschitz condition* $|f_M(t,z,C_1) - f_M(t,z,C_2)| \le L_f |C_1 - C_2|$ *with the constant* $L_f = 2k_\mathrm{b} M$*;*

(b) the function R *is non-decreasing in* C*, satisfies the Lipschitz condition with the constant* $\bar{V}/K_M$*, and* $R(t,z,C)\, C \ge 0$ *for all* C*; for* $C \ge 0$ *it coincides with Monod kinetics (2).*

Proof. (a) For fixed t, z, set $c = C_\mathrm{crit}(t,z) \ge 0$ and $g(y) = k_\mathrm{b}(y-c)^+ y$, $y \in [0,M]$. The function g is continuous, vanishes for $y \le c$, and for $y > c$ has the derivative $g'(y) = k_\mathrm{b}(2y - c) \in [0, 2k_\mathrm{b} M]$; hence it is non-decreasing and Lipschitz continuous with the constant $2k_\mathrm{b} M$, and $0 \le g \le k_\mathrm{b} M^2$. The map Π_M is non-decreasing and Lipschitz continuous with the constant 1, and $f_M = g \circ \Pi_M$. (b) For $C \ge 0$ the derivative of R with respect to C equals $V_\mathrm{max} K_M/(K_M + C)^2 \in [0, V_\mathrm{max}/K_M]$, and for $C < 0$ it equals V_max/K_M; the function R is continuous at zero, which implies its monotonicity and the Lipschitz property. Finally, $R(t,z,C)\, C = V_\mathrm{max} C^2/(K_M + C^+) \ge 0$. □

Lemma 2 (Inequalities for functions in V). *For any* $v \in V$ *and* $z_0 \in [0,L]$*,*

$$|v(z_0)| \le L^{-1/2} \parallel v \parallel + L^{1/2} \parallel \partial_z v \parallel, \qquad \parallel v \parallel^2 \le L^2 \parallel \partial_z v \parallel^2 + 2L\, v(L)^2. \tag{17}$$

Proof. From the representation $v(z_0) = v(z) + \int_z^{z_0} \partial_z v \, d\zeta$ and the Cauchy–Schwarz inequality, $|v(z_0)| \le |v(z)| + L^{1/2} \parallel \partial_z v \parallel$; integrating over $z \in (0,L)$ and dividing by L, we obtain the first inequality, since $\int_0^L |v| \, dz \le L^{1/2} \parallel v \parallel$. From the representation $v(z) = v(L) - \int_z^L \partial_z v \, d\zeta$ and the inequality $(a-b)^2 \le 2a^2 + 2b^2$ it follows that $v(z)^2 \le 2v(L)^2 + 2(L-z) \parallel \partial_z v \parallel^2$; integration over z gives the second inequality. □

3.7.3 Weak formulation

Definition 1. Let $W = \{v \in L^2(0,t_\mathrm{f}; V) \colon \partial_t v \in L^2(0,t_\mathrm{f}; V')\}$. A weak solution of problem (14), (11), (12) with the flux f_M is a function $C \in W$, $C(0) = C_0$, such that for almost all $t \in (0,t_\mathrm{f})$ and all $\varphi \in V$

$$\begin{aligned} &\langle \partial_t C, \varphi \rangle + \int_0^L \big(D\ \partial_z C - f_M(t,z,C) \big)\, \partial_z \varphi \, dz + \int_0^L R\,(t,z,C)\, \varphi \, dz \\ &+ k_\mathrm{atm} C(t,L)\, \varphi(L) + q_\mathrm{p}\, C(t,z_\mathrm{r})\, \varphi(z_\mathrm{r}) = \int_0^L S\ \varphi \, dz + k_\mathrm{atm} C_\mathrm{eq}\, \varphi(L). \end{aligned} \tag{18}$$

Identity (18) is obtained by multiplying (14) by φ and integrating by parts with the boundary conditions (11), (12) taken into account; the flux boundary conditions are natural for it, and the δ-sink turns into the point term $q_\mathrm{p} C(t,z_\mathrm{r}) \varphi(z_\mathrm{r})$. For smooth solutions, the identity is equivalent to the original problem. Since $W \subset C\big([0,t_\mathrm{f}]; L^2(\Omega)\big)$ [34], the initial condition makes sense; by Lemma 2, the values $C(t,L)$ and $C(t,z_\mathrm{r})$ are defined for almost all t without regularization.

The linear part of identity (18) is given by the form

$$a(u,v) = \int_0^L D\ \partial_z u\ \partial_z v \, dz + k_\mathrm{atm} u(L)\, v(L) + q_\mathrm{p}\, u(z_\mathrm{r})\, v(z_\mathrm{r}), \qquad u, v \in V. \tag{19}$$

By Lemma 2, the form a is bounded on $V \times V$, and for $k_\mathrm{atm} > 0$ it is coercive:

$$a(v,v) \geq D_{\min} \parallel \partial_z v \parallel^2 + k_{\text{atm}} v(L)^2 \geq \mu_0 \parallel v \parallel^2, \qquad \mu_0 = \min\left\{\frac{D_{\min}}{L^2}, \frac{k_{\text{atm}}}{2L}\right\}, \tag{20}$$

whence $a(v,v) \geq c_0 \parallel v \parallel_V^2$ with $c_0 = \frac{1}{2}\min\{D_{\min}, \mu_0\}$. Indeed, by the second inequality in (17), $D_{\min} \parallel \partial_z v \parallel^2 + k_{\text{atm}} v(L)^2 \geq \mu_0(L^2 \parallel \partial_z v \parallel^2 + 2Lv(L)^2) \geq \mu_0 \parallel v \parallel^2$.

3.7.4 Existence, uniqueness and non-negativity

Theorem 1. *Let assumptions (A1)–(A3) hold and* $M > \sup_Q C_{\text{crit}}$. *Then there exists a unique weak solution* $C \in W$. *It has the following properties:* $C \in C\big([0,t_{\text{f}}]; L^2(\Omega)\big)$; *for almost all* t, *the function* $C(t,\cdot)$ *is continuous on* $[0,L]$ *and has a square-integrable derivative with respect to* z; $C \geq 0$ *almost everywhere in* Q; *for any* $\gamma > 0$ *the energy estimate*

$$\begin{aligned} &\parallel C(t) \parallel^2 + \int_0^t (D_{\min} \parallel \partial_z C \parallel^2 + k_{\text{atm}} C(s,L)^2)\, ds \\ &\leq e^{2Kt}\left(\parallel C_0 \parallel^2 + \frac{1}{\gamma}\int_0^t \parallel S \parallel^2 ds + k_{\text{atm}} C_{\text{eq}}^2\, t\right), \qquad K = \frac{L_f^2}{2D_{\min}} + \frac{\gamma}{2}, \end{aligned} \tag{21}$$

holds.

Since $C \geq 0$, the extended kinetics coincides with the original one, and C is a solution of the problem with Monod kinetics (2).

Proof. Step 1: Galerkin approximations. Let $\{w_k\}_{k\geq 1}$ be a basis that is orthonormal in $L^2(\Omega)$ and orthogonal in V (for example, the eigenfunctions of the operator $-\partial_{zz}$ with Neumann conditions). The approximate solution $C_m(t) = \sum_{k=1}^m c_k(t) w_k$ is defined by the conditions $\big(C_m(0), w_j\big) = \big(C_0, w_j\big)$ and the equalities

$$\big(\partial_t C_m, w_j\big) + a\big(C_m, w_j\big) - \big(f_M(C_m), \partial_z w_j\big) + \big(R(C_m), w_j\big) = \big(S, w_j\big) + k_{\text{atm}} C_{\text{eq}} w_j(L) \tag{22}$$

for $j = 1, \dots, m$, where $f_M(C_m) = f_M\big(t,\cdot, C_m(t)\big)$ and $R(C_m) = R\big(t,\cdot, C_m(t)\big)$. This is a system of ordinary differential equations for $c_1, \dots, c_m$ whose right-hand side is, by Lemma 1, Lipschitz continuous in c and square integrable in t; it has a unique solution on some interval $(0, t_m)$, and the estimate of Step 2 shows that $t_m = t_{\text{f}}$.

Step 2: a priori estimate. Multiplying (22) by c_j and summing over j, which is equivalent to substituting $\varphi = C_m$ in (18), we obtain

$$\begin{aligned} &\frac{1}{2}\frac{d}{dt}\parallel C_m \parallel^2 + a(C_m, C_m) + (R(C_m), C_m) \\ &= (f_M(C_m), \partial_z C_m) + (S, C_m) + k_{\text{atm}} C_{\text{eq}} C_m(t,L). \end{aligned} \tag{23}$$

By Lemma 1, $(R(C_m), C_m) \geq 0$ and $|f_M(C_m)| \leq L_f |C_m|$; therefore, by Young's inequality, $|(f_M(C_m), \partial_z C_m)| \leq \frac{D_{\min}}{2} \parallel \partial_z C_m \parallel^2 + \frac{L_f^2}{2D_{\min}} \parallel C_m \parallel^2$; furthermore, $(S, C_m) \leq \frac{1}{2\gamma} \parallel S \parallel^2 + \frac{\gamma}{2} \parallel C_m \parallel^2$ and $k_{\text{atm}} C_{\text{eq}} C_m(t,L) \leq \frac{k_{\text{atm}}}{2} C_m(t,L)^2 + \frac{k_{\text{atm}}}{2} C_{\text{eq}}^2$. Taking (20) into account and omitting the term $q_{\text{p}} C_m(t, z_{\text{r}})^2 \geq 0$, we obtain

$$\frac{d}{dt}\parallel C_m \parallel^2 + D_{\min} \parallel \partial_z C_m \parallel^2 + k_{\text{atm}} C_m(t,L)^2 \leq 2K \parallel C_m \parallel^2 + \frac{1}{\gamma} \parallel S \parallel^2 + k_{\text{atm}} C_{\text{eq}}^2. \tag{24}$$

Multiplication by e^{-2Kt}, integration over $(0,t)$ and the estimate $\parallel C_m(0) \parallel \leq \parallel C_0 \parallel$ give (21) for C_m. Hence the sequence $\{C_m\}$ is bounded in $L^\infty\big(0, t_{\text{f}}; L^2(\Omega)\big) \cap L^2(0, t_{\text{f}}; V)$.

Step 3: estimate of the time derivative. Let P_m be the orthogonal projector of V onto $\mathrm{span}\{w_1, \dots, w_m\}$; for the chosen basis, $\| P_m\varphi \|_V \le \| \varphi \|_V$. For $\varphi \in V$, (22) implies $\langle \partial_t C_m, \varphi\rangle = (\partial_t C_m, P_m\varphi)$, and, by Lemma 2 and the boundedness of the form a,

$$|\langle \partial_t C_m, \varphi\rangle| \le c\big(\| C_m \|_V + \| f_M(C_m) \| + \| R(C_m) \| + \| S \| + k_{\mathrm{atm}} C_{\mathrm{eq}}\big) \| \varphi \|_V, \tag{25}$$

where $\| f_M(C_m) \| \le F_M L^{1/2}$ and $\| R(C_m) \| \le (\bar{V}/K_M) \| C_m \|$ by Lemma 1. Therefore, $\{\partial_t C_m\}$ is bounded in $L^2(0, t_\mathrm{f}; V')$.

Step 4: passage to the limit. The embedding $V \subset L^2(\Omega)$ is compact; therefore, by the Aubin–Lions compactness theorem [34], one can extract from $\{C_m\}$ a subsequence that converges to some function $C \in W$ weakly in $L^2(0, t_\mathrm{f}; V)$ and strongly in $L^2(Q)$, and such that $\partial_t C_m \rightharpoonup \partial_t C$ weakly in $L^2(0, t_\mathrm{f}; V')$. Owing to the Lipschitz continuity, $f_M(C_m) \to f_M(C)$ and $R(C_m) \to R(C)$ strongly in $L^2(Q)$. The functionals $v \mapsto v(L)$ and $v \mapsto v(z_\mathrm{r})$ are linear and continuous on V (Lemma 2); therefore, $C_m(\cdot, L) \rightharpoonup C(\cdot, L)$ and $C_m(\cdot, z_\mathrm{r}) \rightharpoonup C(\cdot, z_\mathrm{r})$ weakly in $L^2(0, t_\mathrm{f})$. Multiplying (22) by an arbitrary $\psi \in C^\infty[0, t_\mathrm{f}]$, integrating over t and passing to the limit for fixed j, we obtain (18) with $\varphi = w_j$; since linear combinations of the w_j are dense in V, identity (18) holds for all $\varphi \in V$ for almost all t. The equality $C(0) = C_0$ follows from the convergence $C_m(0) \to C_0$ in $L^2(\Omega)$ after integration by parts in t with $\psi(t_\mathrm{f}) = 0$. Estimate (21) is preserved in the limit owing to the weak lower semicontinuity of the norm. The regularity properties follow from the inclusions $C \in W \subset C\big([0, t_\mathrm{f}]; L^2(\Omega)\big)$ and $C(t,\cdot) \in V \subset C[0, L]$ for almost all t.

Step 5: non-negativity. For $C \in W$, the function $C^- = \min\{C, 0\}$ belongs to $L^2(0, t_\mathrm{f}; V)$, $\partial_z C^- = \partial_z C \cdot \mathbf{1}_{\{C<0\}}$, and $\frac{1}{2}\frac{d}{dt} \| C^- \|^2 = \langle \partial_t C, C^-\rangle$ [34]. Substitute $\varphi = C^-$ in (18). The bubble term vanishes: $f_M(C) = 0$ where $C < 0$, and $\partial_z C^- = 0$ where $C \ge 0$. The remaining terms on the left-hand side are non-negative: the diffusion term equals $\int D\, |\partial_z C^-|^2 dz$, the reaction term $(R(C), C^-) = \int_{\{C<0\}} R(C)\, C\, dz$ is non-negative by Lemma 1, and the boundary and point terms equal $k_{\mathrm{atm}} C^-(t, L)^2$ and $q_\mathrm{p} C^-(t, z_\mathrm{r})^2$. The right-hand side $(S, C^-) + k_{\mathrm{atm}} C_{\mathrm{eq}} C^-(t, L)$ is non-positive by (A2) and (A3). Hence $\frac{d}{dt} \| C^- \|^2 \le 0$, and $C^-(0) = C_0^- = 0$ implies $C^- \equiv 0$, i.e., $C \ge 0$.

Step 6: uniqueness follows from Theorem 2 with coinciding data. □

3.7.5 Continuous dependence on the data

Theorem 2. *Let $C^{(1)}$, $C^{(2)}$ be weak solutions with data $\big(C_0^{(1)}, S^{(1)}\big)$ and $\big(C_0^{(2)}, S^{(2)}\big)$ satisfying (A2), with the same coefficients. Then for all $t \in [0, t_\mathrm{f}]$ and any $\gamma > 0$*

$$\begin{aligned} &\| C^{(1)}(t) - C^{(2)}(t) \|^2 + D_{\min} \int_0^t \| \partial_z\big(C^{(1)} - C^{(2)}\big) \|^2\, ds \\ &\quad \le e^{2Kt}\left(\| C_0^{(1)} - C_0^{(2)} \|^2 + \frac{1}{\gamma} \int_0^t \| S^{(1)} - S^{(2)} \|^2\, ds \right), \end{aligned} \tag{26}$$

where K is defined in (21). In particular, the weak solution is unique, and the problem is well posed in the Hadamard sense in $C\big([0, t_\mathrm{f}]; L^2(\Omega)\big)$.

Proof. For the difference $w = C^{(1)} - C^{(2)} \in W$, substitute $\varphi = w$ in the difference of identities (18):

$$\frac{1}{2}\frac{d}{dt}\parallel w \parallel^2 + a(w,w) + \left(R\left(C^{(1)}\right) - R\left(C^{(2)}\right), w\right) = \left(f_M\left(C^{(1)}\right) - f_M\left(C^{(2)}\right), \partial_z w\right) + \left(S^{(1)} - S^{(2)}, w\right). \tag{27}$$

On the left-hand side, $a(w,w) \geq D_{\min} \parallel \partial_z w \parallel^2$ by (20), and $\left(R\left(C^{(1)}\right) - R\left(C^{(2)}\right)\right) w \geq 0$ owing to the monotonicity of R (Lemma 1). On the right-hand side, by Lemma 1 and Young's inequality, $\left|\left(f_M\left(C^{(1)}\right) - f_M\left(C^{(2)}\right), \partial_z w\right)\right| \leq L_f \parallel w \parallel \parallel \partial_z w \parallel \leq \frac{D_{\min}}{2} \parallel \partial_z w \parallel^2 + \frac{L_f^2}{2D_{\min}} \parallel w \parallel^2$ and $\left(S^{(1)} - S^{(2)}, w\right) \leq \frac{\gamma}{2} \parallel w \parallel^2 + \frac{1}{2\gamma} \parallel S^{(1)} - S^{(2)} \parallel^2$. Hence $\frac{d}{dt} \parallel w \parallel^2 + D_{\min} \parallel \partial_z w \parallel^2 \leq 2K \parallel w \parallel^2 + \frac{1}{\gamma} \parallel S^{(1)} - S^{(2)} \parallel^2$, and Gronwall's lemma yields (26). Only the monotonicity of Monod kinetics has been used; therefore, the estimate does not depend on $V_{\max}$ and K_M and does not deteriorate for small K_M. □

3.7.6 Interface condition at the root uptake level and mass balance

Theorem 3. *Let the assumptions of Theorem 1 hold, let the functions $D(t,\cdot)$ and $C_{\mathrm{crit}}(t,\cdot)$ be continuous on $[0,L]$ for almost all t, and, in addition, let $\partial_t C \in L^2(Q)$. Then for almost all t the total flux $J = -D\,\partial_z C + f_M(t,z,C)$ belongs to $H^1(0,z_\mathrm{r})$ and $H^1(z_\mathrm{r},L)$, Eq. (14) holds almost everywhere in $(0,z_\mathrm{r}) \cup (z_\mathrm{r},L)$, the boundary conditions (11), (12) hold pointwise, and the interface condition*

$$C(t,z_\mathrm{r}-0) = C(t,z_\mathrm{r}+0), \qquad D\left[\frac{\partial C}{\partial z}\right]_{z_\mathrm{r}-0}^{z_\mathrm{r}+0} = q_\mathrm{p}\,C(t,z_\mathrm{r}) \tag{28}$$

is satisfied at the point z_r.

Proof. Fix t for which (18) holds and $\partial_t C(t) \in L^2(\Omega)$. For $\varphi \in C_0^\infty(0,z_\mathrm{r})$ the point and boundary terms in (18) vanish, and the identity takes the form $-\int_0^{z_\mathrm{r}} J\,\partial_z\varphi\,dz = \int_0^{z_\mathrm{r}} (S - R - \partial_t C)\,\varphi\,dz$, i.e., $\partial_z J = S - R - \partial_t C \in L^2(0,z_\mathrm{r})$ in the sense of distributions; hence $J \in H^1(0,z_\mathrm{r})$, and the equation holds almost everywhere. The same argument applies on (z_r,L). Since J is continuous on each of the segments $[0,z_\mathrm{r}]$ and $[z_\mathrm{r},L]$, for an arbitrary $\varphi \in V$ one can integrate by parts on each of them; comparing the result with (18) and noting that the volume terms cancel, we obtain

$$J(t,0)\,\varphi(0) - \left[J(t,L) - k_{\mathrm{atm}}\left(C(t,L) - C_{\mathrm{eq}}\right)\right]\varphi(L) + \left([J]_{z_\mathrm{r}} + q_\mathrm{p} C(t,z_\mathrm{r})\right)\varphi(z_\mathrm{r}) = 0 \tag{29}$$

for all $\varphi \in V$, where $[J]_{z_\mathrm{r}} = J(t,z_\mathrm{r}+0) - J(t,z_\mathrm{r}-0)$ is the jump of the flux. Choosing φ with appropriate values at the points 0, z_r, L, we find $J(t,0) = 0$, $J(t,L) = k_{\mathrm{atm}}\left(C(t,L) - C_{\mathrm{eq}}\right)$ and $[J]_{z_\mathrm{r}} = -q_\mathrm{p} C(t,z_\mathrm{r})$. The function $f_M\left(t,\cdot,C(t,\cdot)\right)$ is continuous at z_r (as a composition of the continuous functions $C_{\mathrm{crit}}(t,\cdot)$, $C(t,\cdot)$ and Π_M), and so is $D(t,\cdot)$; therefore, the jump of J equals $-D\,[\partial_z C]_{z_\mathrm{r}-0}^{z_\mathrm{r}+0}$, which gives the second equality in (28). The continuity of C follows from the embedding $V \subset C[0,L]$. □

The condition $\partial_t C \in L^2(Q)$ is an additional regularity assumption; it holds for classical solutions, and for weak solutions it can be obtained for smoother data (for example, $C_0 \in V$ and coefficients Lipschitz continuous in t) by standard techniques [35]. In this paper, it is simply assumed: the essential consequence of Theorem 3 is that the δ-sink is equivalent to the interface condition (28), i.e., the concentration is continuous at the uptake point, while the diffusive flux has a jump equal to the sink intensity. The sign agrees with the upward orientation of the z axis: above the uptake point the upward flux is smaller by $q_\mathrm{p} C(t,z_\mathrm{r})$, and the concentration profile has a kink

at z_r. Condition (28) is satisfied exactly by the analytical solution of problem A (Sect. 4.2) and by the manufactured solution of Sect. 7.3, which makes it possible to check its implementation in the code.

Corollary 1 (Mass balance for the weak solution). *Under the assumptions of Theorem 1, the function* $M(t) = \int_0^L C\ dz$ *is absolutely continuous and satisfies the balance (15) with* $F_\mathrm{atm} = k_\mathrm{atm}\big(C(t,L) - C_\mathrm{eq}\big)$ *and* $F_\mathrm{plant} = q_\mathrm{p} C(t, z_\mathrm{r})$*; moreover,* $O(t) \geq 0$ *and* $F_\mathrm{plant}(t) \geq 0$.

Proof. Substitute $\varphi \equiv 1 \in V$ in (18): the integral containing $\partial_z \varphi$ vanishes, $\langle \partial_t C, 1\rangle = \frac{d}{dt}(C, 1) = M'(t)$, and (15) follows. The non-negativity of O and F_plant follows from $C \geq 0$ and Lemma 1. □

The bubble flux does not enter the balance explicitly: inside the column it only redistributes methane, at the bottom it vanishes by (11), and at the surface it is included in F_atm.

3.7.7 Stationary problem

Definition 2. Let D, S, V_max, C_crit be independent of t. A stationary weak solution is a function $C_\mathrm{s} \in V$ satisfying identity (18) with $\partial_t C = 0$:

$$a(C_\mathrm{s}, \varphi) + (R(C_\mathrm{s}), \varphi) - (f_M(C_\mathrm{s}), \partial_z \varphi) = (S, \varphi) + k_\mathrm{atm} C_\mathrm{eq} \varphi(L) \qquad \forall \varphi \in V. \tag{30}$$

Theorem 4. *Let the coefficients be independent of* t*, and let assumptions (A1)–(A3) hold and* $M > \sup C_\mathrm{crit}$.

(a) There exists a stationary weak solution $C_\mathrm{s} \geq 0$*, and it satisfies the balance* $P = O_\mathrm{s} + k_\mathrm{atm}\big(C_\mathrm{s}(L) - C_\mathrm{eq}\big) + q_\mathrm{p} C_\mathrm{s}(z_\mathrm{r})$*, where* $O_\mathrm{s} = \int_0^L R\,(z, C_\mathrm{s})\, dz \geq 0$.

(b) If $L_f^2 < \mu_0 D_\mathrm{min}$*, where* μ_0 *is defined in (20), then the stationary solution is unique, and any weak solution of the non-stationary problem with the same coefficients and source converges to it exponentially:*

$$\| C(t) - C_\mathrm{s} \|^2 \leq e^{-\mu t} \| C_0 - C_\mathrm{s} \|^2, \qquad \mu = \mu_0 - \frac{L_f^2}{D_\mathrm{min}} > 0. \tag{31}$$

Proof. (a) For a given $v \in L^2(\Omega)$, consider the problem: find $C \in V$ such that

$$a(C, \varphi) + (R(C), \varphi) = (S, \varphi) + (f_M(v), \partial_z \varphi) + k_\mathrm{atm} C_\mathrm{eq} \varphi(L) \qquad \forall \varphi \in V. \tag{32}$$

The operator $A: V \to V'$, $\langle A(C), \varphi\rangle = a(C, \varphi) + (R(C), \varphi)$, is bounded and continuous (Lemmas 1 and 2) and strongly monotone: $\langle A(C_1) - A(C_2), C_1 - C_2\rangle \geq a(C_1 - C_2, C_1 - C_2) \geq c_0 \| C_1 - C_2 \|_V^2$ by the monotonicity of R and (20). The right-hand side of (32) is a bounded linear functional on V. By the Browder–Minty theorem [34], problem (32) has a unique solution $C = T(v)$. The substitution $\varphi = C$ and Lemma 2 give an estimate independent of v:

$$\| T(v) \|_V \leq \rho = \frac{1}{c_0}\Big(\| S \| + F_M L^{1/2} + k_\mathrm{atm} C_\mathrm{eq}\big(L^{-1/2} + L^{1/2}\big)\Big). \tag{33}$$

The map T is Lipschitz continuous from $L^2(\Omega)$ to V: subtracting identities (32) for v_1 and v_2 and substituting $\varphi = T(v_1) - T(v_2)$, we obtain $c_0 \| T(v_1) - T(v_2) \|_V^2 \leq L_f \| v_1 - v_2 \| \| T(v_1) - T(v_2) \|_V$. Since the embedding $V \subset L^2(\Omega)$ is compact, the set $T\big(L^2(\Omega)\big)$ is relatively compact in $L^2(\Omega)$; its closed convex hull $\mathcal{K}$ is compact and convex, and $T(\mathcal{K}) \subset \mathcal{K}$. By the Schauder theorem [36], the map T has a fixed point $C_\mathrm{s} = T(C_\mathrm{s})$, which is a stationary weak solution. Non-negativity is proved by substituting $\varphi = C_\mathrm{s}^-$ in (30): as in Step 5 of the

proof of Theorem 1, all terms on the left-hand side are non-negative and the right-hand side is non-positive, whence $\int_0^L D\ |\partial_z C_\mathrm{s}^-|^2 dz + k_\mathrm{atm} C_\mathrm{s}^-(L)^2 = 0$, i.e., C_s^- is constant and equal to $C_\mathrm{s}^-(L) = 0$. The balance is obtained by substituting $\varphi \equiv 1$.

(b) Let C be a weak solution of the non-stationary problem, and let $w = C(t) - C_\mathrm{s}$. Subtracting (30) from (18) and substituting $\varphi = w$, we obtain, as in Theorem 2,

$$\frac{1}{2}\frac{d}{dt} \| w \|^2 + D_\mathrm{min} \| \partial_z w \|^2 + k_\mathrm{atm} w(t,L)^2 \le \frac{D_\mathrm{min}}{2} \| \partial_z w \|^2 + \frac{L_f^2}{2D_\mathrm{min}} \| w \|^2. \tag{34}$$

By (20), $\frac{D_\mathrm{min}}{2} \| \partial_z w \|^2 + k_\mathrm{atm} w(t,L)^2 \ge \frac{1}{2}(D_\mathrm{min} \| \partial_z w \|^2 + k_\mathrm{atm} w(t,L)^2) \ge \frac{\mu_0}{2} \| w \|^2$, whence $\frac{d}{dt} \| w \|^2 \le -\mu \| w \|^2$, and (31) follows. If $C_\mathrm{s}^{(1)}$ and $C_\mathrm{s}^{(2)}$ are two stationary solutions, then, taking $C(t) \equiv C_\mathrm{s}^{(1)}$ in (31) (the solution of the non-stationary problem with $C_0 = C_\mathrm{s}^{(1)}$), we obtain $\| C_\mathrm{s}^{(1)} - C_\mathrm{s}^{(2)} \|^2 \le e^{-\mu t} \| C_\mathrm{s}^{(1)} - C_\mathrm{s}^{(2)} \|^2 \to 0$, i.e., $C_\mathrm{s}^{(1)} = C_\mathrm{s}^{(2)}$. □

Condition (b) means that bubble transport does not dominate diffusion: for $\mu_0 = D_\mathrm{min}/L^2$ it is equivalent to $L_f L / D_\mathrm{min} < 1$. With active ebullition in the base regime ($L_f = 2k_\mathrm{b}M \sim 10^{-4}\,\mathrm{m\,s^{-1}}$, $D \sim 10^{-9}\,\mathrm{m^2\,s^{-1}}$) this condition is not satisfied, and the uniqueness of the stationary regime is not guaranteed by Theorem 4; in the computations, however, the same stationary regime was always obtained for different initial data. For $k_\mathrm{b} = 0$, the relaxation rate is $\mu = \mu_0 = D/L^2 \sim 10^{-9}\,\mathrm{s^{-1}}$: diffusion alone would provide relaxation only over decades. In fact, relaxation is accelerated by oxidation and plant uptake, whose contribution was neglected in estimate (31).

3.7.8 Bubble flux through the surface

Theorem 5. *Let the assumptions of Theorem 4(a) hold, let the function C_crit be continuous on $[0, L]$, let C_s be a stationary weak solution, and let*

$$k_\mathrm{atm}\big(C_\mathrm{crit}(L) - C_\mathrm{eq}\big) > P = \int_0^L S\ dz. \tag{35}$$

Then $C_\mathrm{s}(L) \le C_\mathrm{eq} + P/k_\mathrm{atm} < C_\mathrm{crit}(L)$ and, consequently, $f_M\big(L, C_\mathrm{s}(L)\big) = 0$: in the stationary regime, the bubble flux through the surface vanishes. Moreover, there exists $\varepsilon > 0$ such that ebullition is inactive in the layer $(L - \varepsilon, L]$, and if, in addition, D is continuous, then the flux through the surface is purely diffusive and $F_\mathrm{atm} = -D\ \partial_z C_\mathrm{s}(L) = k_\mathrm{atm}\big(C_\mathrm{s}(L) - C_\mathrm{eq}\big) \le P$.

Proof. By Theorem 4(a), $k_\mathrm{atm}\big(C_\mathrm{s}(L) - C_\mathrm{eq}\big) = P - O_\mathrm{s} - q_\mathrm{p} C_\mathrm{s}(z_\mathrm{r}) \le P$, since $O_\mathrm{s} \ge 0$ and $C_\mathrm{s} \ge 0$; together with (35), this gives $C_\mathrm{s}(L) < C_\mathrm{crit}(L)$ and $f_M\big(L, C_\mathrm{s}(L)\big) = 0$ by Lemma 1. The functions C_s and C_crit are continuous; therefore, the inequality $C_\mathrm{s} < C_\mathrm{crit}$ holds in some neighbourhood of the point L. In the stationary case $\partial_t C = 0$, and the assumptions of Theorem 3 are satisfied automatically, whence $J(L) = -D\ \partial_z C_\mathrm{s}(L) = k_\mathrm{atm}\big(C_\mathrm{s}(L) - C_\mathrm{eq}\big)$. □

Remark 1. In the base regime (Table 1, $T = T_\mathrm{ref}$, $H_\mathrm{w} = 0$), the threshold is $C_\mathrm{crit}(L) \approx 0.99\,\mathrm{mol\,m^{-3}}$ and $k_\mathrm{atm}\big(C_\mathrm{crit}(L) - C_\mathrm{eq}\big) \approx 6.3 \cdot 10^{-6}\,\mathrm{mol\,m^{-2}\,s^{-1}}$, so condition (35) holds with a margin of a factor of about 63; it would be violated only for a production above $\approx 365\,\mathrm{mg\,CH_4\,m^{-2}\,h^{-1}}$, which is two orders of magnitude larger than the observed fluxes. Theorem 5 is a property of the adopted formulation rather than of the numerical

method: under the Robin condition (12) for the total flux, all methane reaching the surface passes through the limited conductance k_{atm}, and bubbles serve only as a fast internal transport pathway; the methane they deliver dissolves below the surface and is then oxidized, taken up by plants or released through mass exchange. If, instead, the boundary condition lets the bubble flux escape freely to the atmosphere and limits only the diffusive component by mass exchange, the conclusion of the theorem does not hold. The theorem does not rule out bubble emission from real mires or in non-stationary regimes, for example, when the atmospheric pressure falls [29].

Remark 2 (On removing the truncation). If the solution of the problem with the flux f_M satisfies $C \le M$ in Q, then $f_M(C) = f(C)$, and C is a weak solution of the original problem (14), (11), (12); by Theorem 2, it does not depend on the choice of $M' \ge M$. Therefore, the truncation does not affect the computations if M exceeds the maximum of the numerical solution; this condition is checked a posteriori and was satisfied in all computations. An a priori uniform bound that would allow one to dispense with the truncation requires a separate analysis of the quadratic bubble flux near the surface and is not considered here.

3.7.9 Summary of the mathematical analysis

Under assumptions (A1)–(A3), the initial–boundary value problem (14), (11), (12) with the truncated bubble flux has a unique weak solution, which is non-negative, continuous in time in $L^2(\Omega)$ and in depth for almost all t, and depends continuously on the initial data and the source (Theorems 1 and 2). The point plant sink is well defined without regularization and is equivalent to the interface condition (28) (Theorem 3); the weak solution satisfies the integral mass balance (Corollary 1). A non-negative stationary solution exists and, for weak bubble transport, is unique and exponentially stable (Theorem 4); under condition (35), bubbles do not escape through the surface (Theorem 5). These properties determine the requirements for the numerical scheme of Sect. 5: it must be conservative (exact discrete mass balance) and monotone (non-negativity of the solution for non-negative data), and it must integrate the δ-sink over the control volume exactly, without regularization; the interface condition (28) and the mass balance serve as independent checks of the implementation.

4 Analytical steady-state solutions for verification

4.1 Test problems

For verification, steady-state analytical solutions of problem (14) are obtained for $D = \mathrm{const}$, $k_{\mathrm{b}} = 0$, linear oxidation (3) and a piecewise constant source. Problem A tests the boundary conditions and the point sink, but not ebullition; problem B tests the resolution of a thin internal layer. The test parameters are listed in Table 2.

Table 2 Parameters of verification problems A and B

Parameter	Problem A	Problem B
L, m	1.0	1.0
z_{s} (source boundary), m	0.8	0.5
z_{r}, m	0.5	– (no sink)
D, m² s⁻¹	10^{-9}	10^{-9}

S_0, mol m⁻³ s⁻¹	$2 \cdot 10^{-8}$	10^{-6}
k, s⁻¹	10^{-7} for $z > z_s$, 0 for $z < z_s$	10^{-5} everywhere
q_p, m s⁻¹	$2 \cdot 10^{-8}$	0
Top boundary condition	Robin: $k_{atm} = 6.4 \cdot 10^{-6}$ m s⁻¹, $C_{eq} = 3.3 \cdot 10^{-6}$ mol m⁻³	Dirichlet: $C(L) = C_L = 0$
$\lambda = \sqrt{k/D}$, m⁻¹	10	100
Dimensionless parameter	$\lambda(L - z_s) = 2$	$\lambda L = 100$

4.2 Problem A: three-zone solution

The steady-state equation of problem A

$$D\,C'' + S_0\,\mathbf{1}_{\{z \le z_s\}} - k\,\mathbf{1}_{\{z > z_s\}}\,C - q_p\,C(z_r)\,\delta(z - z_r) = 0, \qquad 0 < z < L, \tag{36}$$

is solved with the conditions $C'(0) = 0$, $-DC'(L) = k_{atm}\big(C(L) - C_{eq}\big)$. Denote $C_r = C(z_r)$, $B = C(L)$, $d = L - z_s$, $\lambda = \sqrt{k/D}$, and let $Bi = k_{atm}/(D\lambda)$ be the Biot number. Integration over the zones with the interface condition at z_r taken into account gives

$$C(z) = C_r + \frac{S_0}{2D}(z_r^2 - z^2), \qquad 0 \le z \le z_r, \tag{37}$$

$$C(z) = C_r - \frac{S_0}{2D}(z^2 - z_r^2) + \frac{q_p C_r}{D}(z - z_r), \qquad z_r \le z \le z_s, \tag{38}$$

$$C(z) = B\cosh\lambda(L - z) + Bi\,\big(B - C_{eq}\big)\sinh\lambda(L - z), \qquad z_s \le z \le L, \tag{39}$$

where the constants B and C_r are found from a linear system expressing the continuity of the concentration and the flux at the point z_s.

For the parameters of Table 2 ($\lambda d = 2$, $Bi = 640$), $C_r = 0.60959$ mol m⁻³ and $B = 1.612 \cdot 10^{-4}$ mol m⁻³; of the production $P = S_0 z_s$, 76.2% is taken up by plants ($F_{plant} = q_p C_r$), 17.5% is oxidized, and 6.3% escapes to the atmosphere ($F_{atm} = k_{atm}\big(B - C_{eq}\big)$). At z_r the profile has a kink with a local minimum, and at $z_m = q_p C_r / S_0 = 0.610$ m it has a maximum. For $q_p = 0$ and $C_{eq} = 0$, the fraction of methane passing through the oxidized layer, $F_{atm}/P = (\cosh\lambda d + Bi^{-1}\sinh\lambda d)^{-1}$, is determined by the Thiele modulus λd. In this synthetic test, the concentration near the bottom reaches 3.1 mol m⁻³; the excess over the threshold indicates that ebullition has to be tested separately in the full model.

4.3 Problem B (stiff test)

Problem B reads $D\,C'' - kC + S_0\mathbf{1}_{\{z \le z_s\}} = 0$, $C'(0) = 0$, $C(L) = C_L$. Its solution

$$C(z) = \frac{S_0}{k} + C_L\frac{\cosh\lambda z}{\cosh\lambda L} - \frac{S_0}{k}\frac{\cosh\lambda(L - z_s)\cosh\lambda z}{\cosh\lambda L}, \qquad 0 \le z \le z_s, \tag{40}$$

$$C(z) = \frac{S_0}{k}\frac{\sinh\lambda z_s \sinh\lambda(L - z)}{\cosh\lambda L} + C_L\frac{\cosh\lambda z}{\cosh\lambda L}, \qquad z_s \le z \le L, \tag{41}$$

has the form of a step ($C \approx S_0/k = 0.1$ mol m⁻³ at the bottom and $C \approx 0$ at the top) with a transition layer of thickness $\lambda^{-1} = 1$ cm; for $\lambda L = 100$, the ratios of hyperbolic cosines are computed as $e^{x-y}(1 + e^{-2x})/(1 +$

e^{-2y}). The flux through the surface is negligible; therefore, the integral check $\int_0^L C\ dz = (S_0 z_\mathrm{s} - F_\mathrm{atm})/k$ is satisfied by a conservative scheme for any error of the profile and does not serve as a measure of accuracy.

5 Numerical scheme

5.1 Grid and control volumes

On the uniform grid $z_i = ih$, $h = L/N$, with the control volumes $V_i = \left[z_{i-1/2}, z_{i+1/2}\right] \cap [0, L]$ of length h_i ($h/2$ at the boundaries), where $z_\mathrm{r} = z_{j_\mathrm{r}}$ is a grid node, balance (9) is written exactly:

$$h_i \frac{d\bar{C}_i}{dt} + J_{i+1/2} - J_{i-1/2} = h_i(\bar{S}_i - \bar{R}_i) - q_\mathrm{p}\, C(t, z_\mathrm{r})\, \delta_{i,j_\mathrm{r}}. \tag{42}$$

The bar denotes the average over the control volume, and $\delta_{i,j}$ is the Kronecker delta. The boundary fluxes are given by conditions (11), (12); the δ-sink is integrated exactly, and the sources and oxidation are integrated by Gauss–Legendre quadrature with the integration intervals split at the discontinuities of the coefficients.

5.2 Flux approximation

The flux through a face is approximated by the exponential fitting scheme (Il'in's scheme, also known as the Scharfetter–Gummel scheme) [37, 38], which is exact for $-DC' + uC = \mathrm{const}$:

$$\begin{gathered} J_{i+1/2} = \frac{D_{i+1/2}}{h}\left[\mathcal{B}\left(-P_{i+1/2}\right) C_i - \mathcal{B}\left(P_{i+1/2}\right) C_{i+1}\right], \\ P_{i+1/2} = \frac{u_{i+1/2}\, h}{D_{i+1/2}}, \qquad \mathcal{B}(x) = \frac{x}{e^x - 1}. \end{gathered} \tag{43}$$

As $P \to 0$, it reduces to the second-order central difference [39], and for $P \gg 1$ to the upwind difference; the factors $\mathcal{B}(\pm P)$ are positive for any P, and the scheme is monotone. The Péclet number of bubble transport $Pe_f = k_\mathrm{b} C_\mathrm{crit} h/D$ equals 25 for the base parameters and $h = 2.5$ mm, and the central evaluation of the velocity produces checkerboard oscillations at the ebullition front (up to 3% of C_crit). Therefore, the velocity is evaluated in the upwind manner,

$$u_{i+1/2} = k_\mathrm{b} \max\left\{C_i - C_\mathrm{crit}\left(z_{i+1/2}\right),\, 0\right\}, \tag{44}$$

which removes the oscillations at the cost of first-order approximation of the bubble flux (Sect. 7.3).

5.3 Time discretization and solution of the nonlinear system

The implicit Euler scheme is used:

$$\begin{gathered} h_i \frac{C_i^{n+1} - C_i^n}{\tau} + J_{i+1/2}^{n+1} - J_{i-1/2}^{n+1} \\ = h_i \left(\bar{S}_i^{n+1} - \bar{V}_i^{n+1} \frac{C_i^{n+1}}{K_M + C_i^{n+1}}\right) - q_\mathrm{p}\, C_{j_r}^{n+1}\, \delta_{i,j_\mathrm{r}}, \qquad i = 0, \ldots, N. \end{gathered} \tag{45}$$

The nonlinear system is solved by Newton's method with the exact tridiagonal Jacobian and step damping (2–5 iterations for a tolerance of 10^{-11}); stationary regimes are found by pseudo-time marching with step doubling, followed by a final Newton solve with $\tau = \infty$. The algorithm is implemented in MATLAB.

5.4 Properties of the scheme

Proposition 1. *Summation of (45) over i gives an exact discrete analogue of balance (15):*

$$\frac{M_h^{n+1} - M_h^n}{\tau} = P_h^{n+1} - O_h^{n+1} - k_{\mathrm{atm}}\left(C_N^{n+1} - C_{\mathrm{eq}}\right) - q_{\mathrm{p}}\, C_{j_r}^{n+1}, \qquad M_h = \sum_{i=0}^{N} h_i\, C_i, \tag{46}$$

where $P_h = \sum h_i \bar{S}_i$ and $O_h = \sum h_i \bar{R}_i$.

In the computations, the residual of (46) did not exceed $1.1 \cdot 10^{-12} P$.

Proposition 2. *If $C^n \geq 0$, $\bar{S}^{n+1} \geq 0$ and $C_{\mathrm{eq}} \geq 0$, then the numerical solution satisfies $C^{n+1} \geq 0$ owing to the properties of M-matrices [39].*

The verified orders of convergence are the second order in h for $u = 0$, the first order in zones of active ebullition, and the first order in τ.

6 Comparison of analytical and numerical solutions

6.1 Error norms

The accuracy is assessed by the root-mean-square norm $E_2 = \left(\sum_i e_i^2 / (N+1)\right)^{1/2}$ and the maximum norm $E_\infty = \max_i |e_i|$ of the error and by the relative errors of the fluxes $\delta_F = |F^{\mathrm{num}} - F^{\mathrm{an}}| / |F^{\mathrm{an}}|$. Unlike the integral balance check, these measures reveal profile errors near the boundaries and at the root uptake level [40].

6.2 Problem A

Table 3 Comparison of the numerical ($N = 100$) and analytical solutions of problem A

Quantity	Numerical solution	Analytical solution	Relative error
$C(z_{\mathrm{r}})$, mol m^{-3}	0.609540	0.609594	$-8.8 \cdot 10^{-5}$
$C(L)$, mol m^{-3}	$1.6139 \cdot 10^{-4}$	$1.6121 \cdot 10^{-4}$	$1.1 \cdot 10^{-3}$
F_{plant}, mol m^{-2} s^{-1}	$1.21908 \cdot 10^{-8}$	$1.21919 \cdot 10^{-8}$	$-8.8 \cdot 10^{-5}$
F_{atm}, mol m^{-2} s^{-1}	$1.0117 \cdot 10^{-9}$	$1.0107 \cdot 10^{-9}$	$1.1 \cdot 10^{-3}$
O, mol m^{-2} s^{-1}	$2.79745 \cdot 10^{-9}$	$2.79747 \cdot 10^{-9}$	$-6.8 \cdot 10^{-6}$
Residual of balance (46), fraction of P	$1.6 \cdot 10^{-15}$	0	–

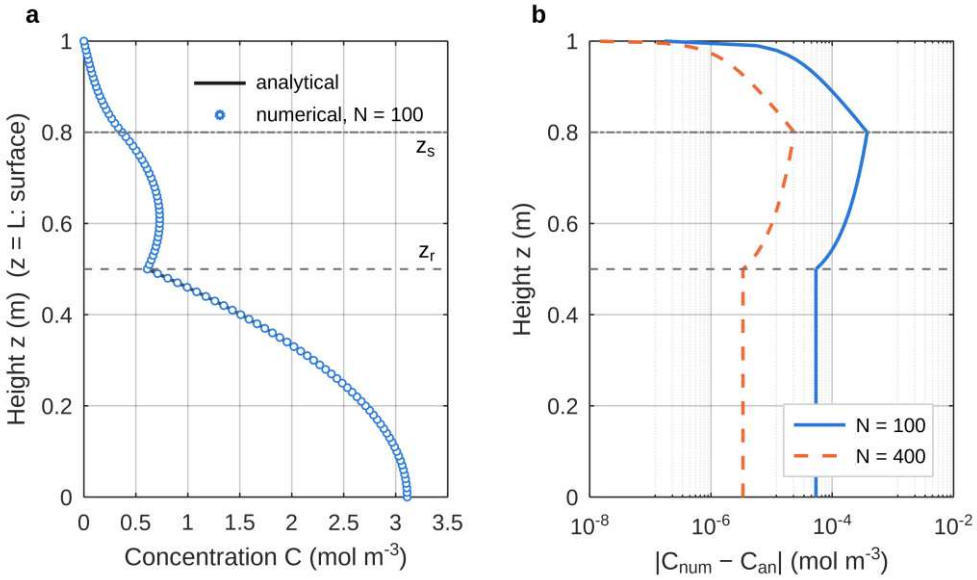


Fig. 2 Problem A: **a** analytical solution (37)–(39) and numerical solution for $N = 100$; **b** profiles of the absolute error for $N = 100$ and $N = 400$. Dashed line: root uptake level z_r; dash-dotted line: boundary z_s of the oxidation zone; the z axis points upward, and $z = L$ is the surface

For $N = 100$ ($h = 1$ cm), the numerical solution reproduces all features of the analytical one (Table 3, Fig. 2): the parabola below the uptake point, the kink at z_r, the flux divide at z_m and the exponential decay in the oxidized layer. The fluxes are reproduced with an error not exceeding $1.1 \cdot 10^{-3}$, and the balance to machine precision; the error is maximal at the discontinuity point z_s of the oxidation coefficient and decreases by a factor of 16 at all points when the number of nodes is quadrupled.

6.3 Problem B

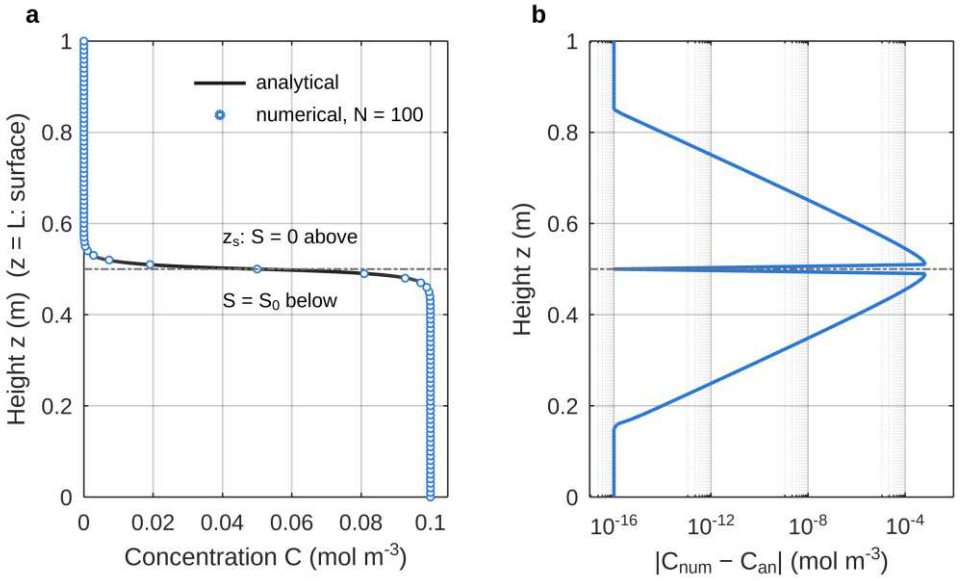


Fig. 3 Problem B (stiff test): **a** analytical (40)–(41) and numerical ($N = 100$) solutions; **b** profile of the absolute error. The z axis points upward ($z = L$ is the surface)

For $N = 100$ ($\lambda h = 1$), $E_2 = 1.33 \cdot 10^{-4}$ and $E_\infty = 7.04 \cdot 10^{-4}$ mol m^{-3}, while the integral $\int_0^L C\ dz$ coincides with the exact value to all seven significant digits. The error is concentrated in the transition layer, which contains only two or three nodes, and outside it decreases as $e^{-\lambda|z-z_s|}$ down to machine precision (Fig. 3).

7 Convergence study

7.1 Methodology

The order of convergence is estimated on nested grids from the change of the error norm when the number of intervals is doubled and by regression over the asymptotic range [40].

7.2 Problems A and B

Table 4 Convergence of the numerical solutions of problems A and B ($h = L/N$, $L = 1$ m)

	Problem A				Problem B	
N	E_2, mol m^{-3}	$p_{2,j}$	$\delta_{F_{atm}}$	λh	E_2, mol m^{-3}	$p_{2,j}$
20	$3.630 \cdot 10^{-3}$	1.892	$2.7 \cdot 10^{-2}$	5.00	$4.688 \cdot 10^{-4}$	–
40	$9.301 \cdot 10^{-4}$	1.964	$6.7 \cdot 10^{-3}$	2.50	$4.620 \cdot 10^{-4}$	0.021
80	$2.347 \cdot 10^{-4}$	1.987	$1.7 \cdot 10^{-3}$	1.25	$1.947 \cdot 10^{-4}$	1.247
160	$5.888 \cdot 10^{-5}$	1.995	$4.2 \cdot 10^{-4}$	0.63	$5.539 \cdot 10^{-5}$	1.814
320	$1.475 \cdot 10^{-5}$	1.998	$1.1 \cdot 10^{-4}$	0.31	$1.425 \cdot 10^{-5}$	1.959
640	$3.689 \cdot 10^{-6}$	1.999	$2.6 \cdot 10^{-5}$	0.16	$3.587 \cdot 10^{-6}$	1.990
1280	$9.226 \cdot 10^{-7}$	2.000	$6.6 \cdot 10^{-6}$	0.08	$8.983 \cdot 10^{-7}$	1.997

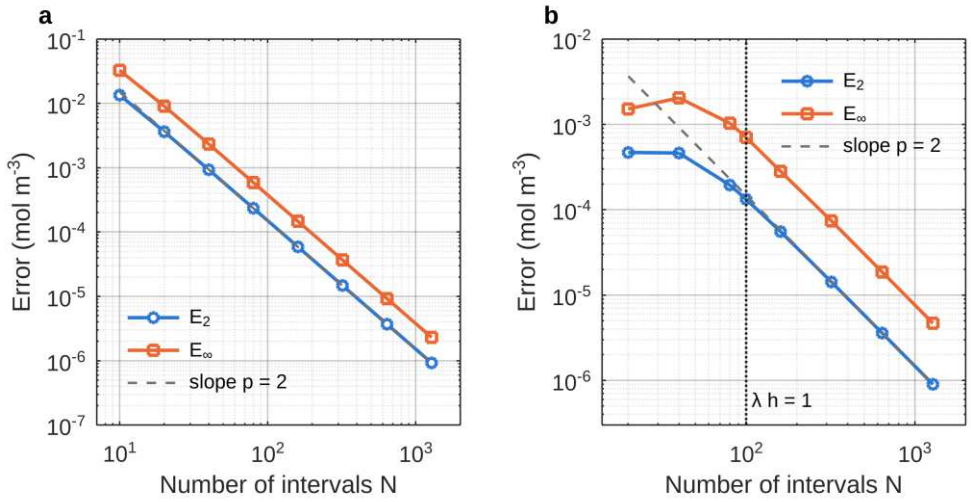


Fig. 4 Convergence of the numerical solutions: **a** problem A; **b** problem B. Dashed line: second-order reference slope $p = 2$; dotted line in panel **b**: the boundary $\lambda h = 1$ beyond which the asymptotic range begins

For problem A, regression over the points $N \geq 80$ gives $p_2 = 1.998$ and $p_\infty = 1.999$; second order is observed already at $N = 20$ and is preserved for the fluxes, i.e., the exact integration of the δ-sink, the averaging of discontinuous coefficients and the approximation of the Robin condition do not reduce the order. For problem B, regression over the points $N \geq 160$ gives $p_2 = 1.983$ and $p_\infty = 1.974$; the asymptotic range begins at $\lambda h < 1$, i.e., resolving a layer of thickness λ^{-1} requires $h < \lambda^{-1}$ (Table 4, Fig. 4).

7.3 Full nonlinear unsteady scheme: method of manufactured solutions

Bubble transport, nonlinear oxidation, variable D and time dependence are tested by the method of manufactured solutions [40]. For the prescribed solution

$$C_{\mathrm{mms}}(z,t) = \theta(t)(1 + 0.6\cos\pi z) + 0.4z^2 + \psi(t)\,|z - z_{\mathrm{r}}|,$$
$$\theta(t) = 1 + 0.5\sin 2\pi t, \qquad \psi(t) = \frac{q_{\mathrm{p}}\, C_{\mathrm{mms}}(z_{\mathrm{r}}, t)}{2D(z_{\mathrm{r}})}, \tag{47}$$

which satisfies the interface condition (28) exactly, the source is computed by substitution into the equation, and the numerical solution is compared with the prescribed one ($D = 1 + 0.5z$, $V_{\max} = 1 + z$, $C_{\mathrm{crit}} = 1.2 + 0.3(1 - z)$, $q_{\mathrm{p}} = 0.8$, $k_{\mathrm{b}} \in \{0,\ 0.5\}$; for $k_{\mathrm{b}} = 0.5$, ebullition is active in part of the domain).

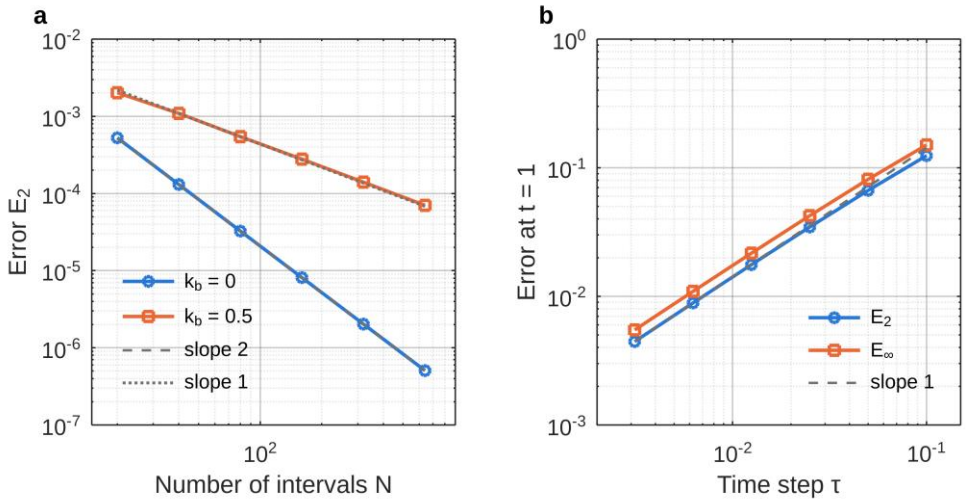


Fig. 5 Method of manufactured solutions: **a** spatial convergence without ebullition ($k_\mathrm{b} = 0$, second order) and with active ebullition ($k_\mathrm{b} = 0.5$, first order), dashed and dotted lines are the second- and first-order reference slopes; **b** temporal convergence for $N = 800$ (first order), the dashed line is the first-order reference slope

The spatial order equals 2.00 for $k_\mathrm{b} = 0$ and 0.99 for $k_\mathrm{b} = 0.5$ (Fig. 5a); the first order under active ebullition is a consequence of the upwind evaluation of the velocity (44). The temporal order equals 0.99 (Fig. 5b), as expected for the implicit Euler scheme.

7.4 Verification summary

The observed orders of convergence agree with the theoretical ones, and the mass balance holds to machine precision.

8 Conclusions

1. A one-dimensional model of methane dynamics in water-saturated peat with methanogenesis, oxidation, diffusion, ebullition and plant-mediated transport is constructed. Compared with the Walter–Heimann model [10], the following elements are modified: the ebullition threshold, which depends on depth, temperature and pressure instead of being constant; the description of transport, in which ebullition is specified by a continuous flux when the threshold is exceeded and plant uptake by a point sink at the root uptake level; and the boundary condition at the surface, where a condition of exchange with the atmosphere (Robin condition) is adopted instead of a prescribed concentration. Individual elements of these approaches are known [12, 13, 16, 17]; the contribution of this paper lies in combining them in a single formulation and analysing it mathematically and numerically.
2. Under the stated assumptions, the existence, uniqueness and non-negativity of the weak solution and its continuous dependence on the data are proved for the truncated bubble flux. The point sink is well defined in the one-dimensional problem; the stationary bubble flux through the surface vanishes whenever $k_\mathrm{atm}\big(C_\mathrm{crit}(L) - C_\mathrm{eq}\big) > P$, which is a property of the adopted formulation.
3. Analytical solutions for two test regimes are obtained; together with the method of manufactured solutions, they confirmed mass conservation, second-order spatial convergence of the scheme without active ebullition, and first-order convergence with active bubble transport and in time.

4. The verified algorithm can be used to compute methane emission in scenarios for West Siberian mires; quantitative estimates will require calibration of the adopted parameters.

The model does not separately resolve the gas phase, the dynamics of the water table and oxygen, freezing and thawing, or changes in plant-mediated transport. The assumed values of P, ℓ_S, q_p and z_r require independent calibration against field measurements of methane fluxes [6]. Further development of the model involves a two-phase description of ebullition [29, 30] and accounting for the dynamics of the water table and oxygen, freezing and thawing.

ORCID iDs

Sergey P. Semenov: https://orcid.org/0000-0001-8432-9767; Artem O. Tashkin: https://orcid.org/0000-0002-8231-8703.

Acknowledgements

The study was supported by the Russian Science Foundation, project No. 25-11-20026, https://rscf.ru/project/25-11-20026/.

Declarations

- **Funding.** This work was supported by the Russian Science Foundation, project No. 25-11-20026.
- **Competing interests.** The authors declare no competing interests.
- **Ethics approval and consent to participate.** Not applicable.
- **Consent for publication.** Not applicable.
- **Data availability.** All data needed to reproduce the results (model parameters and test problem settings) are given in the paper; the computed results are available from the corresponding author upon reasonable request.
- **Materials availability.** Not applicable.
- **Code availability.** The MATLAB code is available from the corresponding author upon reasonable request.
- **Author contribution.** Sergey P. Semenov: Conceptualization, Methodology, Formal analysis (well-posedness results of Sect. 3.7), Writing – original draft, Supervision. Artem O. Tashkin: Methodology, Software (MATLAB implementation), Validation (analytical test problems, convergence study and method of manufactured solutions, Sects. 4–7), Visualization, Writing – review and editing. All authors read and approved the final manuscript.

References

[1] Saunois, M., Martinez, A., Poulter, B., *et al.*: Global methane budget 2000–2020. Earth Syst. Sci. Data **17**(5), 1873–1958 (2025) https://doi.org/10.5194/essd-17-1873-2025

[2] Lai, D.Y.F.: Methane dynamics in northern peatlands: a review. Pedosphere **19**(4), 409–421 (2009) https://doi.org/10.1016/S1002-0160(09)00003-4

[3] Bridgham, S.D., Cadillo-Quiroz, H., Keller, J.K., Zhuang, Q.: Methane emissions from wetlands: biogeochemical, microbial, and modeling perspectives from local to global scales. Glob. Change Biol. **19**(5), 1325–1346 (2013) https://doi.org/10.1111/gcb.12131

[4] Ge, M., Korrensalo, A., Laiho, R., *et al.*: Plant-mediated CH_4 exchange in wetlands: a review of mechanisms and measurement methods with implications for modelling. Sci. Total Environ. **914**, 169662 (2024) https://doi.org/10.1016/j.scitotenv.2023.169662

[5] Glagolev, M., Kleptsova, I., Filippov, I., *et al.*: Regional methane emission from West Siberia mire landscapes. Environ. Res. Lett. **6**(4), 045214 (2011) https://doi.org/10.1088/1748-9326/6/4/045214

[6] Dyukarev, E.A., Veretennikova, E.E., Sabrekov, A.F., *et al.*: Methane and carbon dioxide fluxes correlation according to automatic chamber observations at the Mukhrino bog ridge and hollow complex. Environ. Dyn. Glob. Clim. Change **15**(4), 276–288 (2024) https://doi.org/10.18822/edgcc636456

[7] Veretennikova, E.E., Dyukarev, E.A.: Spatiotemporal variability of methane emission in oligotrophic ridge–hollow complexes of Western Siberia (in Russian). Izv. Ross. Akad. Nauk, Ser. Geogr. **89**(2), 297–312 (2025) https://doi.org/10.31857/S2587556625020118

[8] Glagolev, M.V., Sabrekov, A.F., Kleptsova, I.E., *et al.*: Methane emission from bogs in the subtaiga of Western Siberia: the development of standard model. Eurasian Soil Sci. **45**(10), 947–957 (2012) https://doi.org/10.1134/S106422931210002X

[9] Golovatskaya, E.A., Veretennikova, E.E., Dyukarev, E.A.: Greenhouse gas fluxes and carbon sequestration in the oligotrophic peat soils of southern taiga in Western Siberia. Eurasian Soil Sci. **57**(2), 210–219 (2024) https://doi.org/10.1134/S1064229323602871

[10] Walter, B.P., Heimann, M.: A process-based, climate-sensitive model to derive methane emissions from natural wetlands: application to five wetland sites, sensitivity to model parameters, and climate. Glob. Biogeochem. Cycles **14**(3), 745–765 (2000) https://doi.org/10.1029/1999GB001204

[11] Bohn, T.J., Podest, E., Schroeder, R., *et al.*: Modeling the large-scale effects of surface moisture heterogeneity on wetland carbon fluxes in the West Siberian Lowland. Biogeosciences **10**(10), 6559–6576 (2013) https://doi.org/10.5194/bg-10-6559-2013

[12] Wania, R., Ross, I., Prentice, I.C.: Implementation and evaluation of a new methane model within a dynamic global vegetation model: LPJ-WHyMe v1.3.1. Geosci. Model Dev. **3**(2), 565–584 (2010) https://doi.org/10.5194/gmd-3-565-2010

[13] Riley, W.J., Subin, Z.M., Lawrence, D.M., *et al.*: Barriers to predicting changes in global terrestrial methane fluxes: analyses using CLM4Me, a methane biogeochemistry model integrated in CESM. Biogeosciences **8**(7), 1925–1953 (2011) https://doi.org/10.5194/bg-8-1925-2011

[14] Kaiser, S., Göckede, M., Castro-Morales, K., *et al.*: Process-based modelling of the methane balance in periglacial landscapes (JSBACH-methane). Geosci. Model Dev. **10**(1), 333–358 (2017) https://doi.org/10.5194/gmd-10-333-2017

[15] Raivonen, M., Smolander, S., Backman, L., *et al.*: HIMMELI v1.0: HelsinkI model of MEthane buiLd-up and emIssion for peatlands. Geosci. Model Dev. **10**(12), 4665–4691 (2017) https://doi.org/10.5194/gmd-10-4665-2017

[16] Stepanenko, V.M., Machul'skaya, E.E., Glagolev, M.V., Lykossov, V.N.: Numerical modeling of methane emissions from lakes in the permafrost zone. Izv. Atmos. Ocean. Phys. **47**(2), 252–264 (2011) https://doi.org/10.1134/S0001433811020113

[17] Morel, X., Decharme, B., Delire, C., *et al.*: A new process-based soil methane scheme: evaluation over Arctic field sites with the ISBA land surface model. J. Adv. Model. Earth Syst. **11**(1), 293–326 (2019) https://doi.org/10.1029/2018MS001329

[18] Peltola, O., Raivonen, M., Li, X., *et al.*: Technical note: comparison of methane ebullition modelling approaches used in terrestrial wetland models. Biogeosciences **15**(3), 937–951 (2018) https://doi.org/10.5194/bg-15-937-2018

[19] Bohn, T.J., Melton, J.R., Ito, A., *et al.*: WETCHIMP-WSL: intercomparison of wetland methane emissions models over West Siberia. Biogeosciences **12**(11), 3321–3349 (2015) https://doi.org/10.5194/bg-12-3321-2015

[20] Semenov, S.P., Tashkin, A.O.: The carbon cycle models analysis as applied to research of wetland ecosystems in Western Siberia (in Russian). Yugra State Univ. Bull. **18**(4), 145–152 (2022) https://doi.org/10.18822/byusu202204145-152

[21] Dyukarev, E.A., Semenov, S.P.: Numerical modeling of biogeochemical carbon cycles in swamp ecosystems (in Russian). Izv. Altai State Univ. **4(126)**, 104–109 (2022) https://doi.org/10.14258/izvasu(2022)4-16

[22] Semenov, S.P., Dyukarev, E.A., Tashkin, A.O.: Mathematical model for calculating carbon dynamics in wetland ecosystems of cold regions of Western Siberia (in Russian). Math. Notes NEFU **31**(1), 102–115 (2024) https://doi.org/10.25587/2411-9326-2024-1-102-115

[23] Tukmacheva, Y.A., Pyatkov, S.G.: Numerical solution of the inverse problem of identifying the methane consumption rate in soil (in Russian). Yugra State Univ. Bull. **20**(4), 74–81 (2024) https://doi.org/10.18822/byusu20240474-81

[24] Tukmacheva, Y.A., Pyatkov, S.G.: Identification of the absorption parameter in convection–diffusion equations (in Russian). Chelyab. Phys. Math. J. **10**(4), 701–714 (2025) https://doi.org/10.47475/2500-0101-2025-10-4-701-714

[25] Kotsyurbenko, O.R., Da Silva, A.P., Glagolev, M.V.: Methanogenic microbial community from the peat bog "Chistoe" (West Siberia): preliminary data and perspectives (in Russian). Environ. Dyn. Glob. Clim. Change **1**(1S), 136–140 (2008) https://doi.org/10.17816/edgcc11S136-140

[26] Beckmann, M., Lloyd, D.: Mass spectrometric monitoring of gases (CO_2, CH_4, O_2) in a mesotrophic peat core from Kopparås Mire, Sweden. Glob. Change Biol. **7**(2), 171–180 (2001) https://doi.org/10.1046/j.1365-2486.2001.00396.x

[27] Sander, R.: Compilation of Henry's law constants (version 5.0.0) for water as solvent. Atmos. Chem. Phys. **23**(19), 10901–12440 (2023) https://doi.org/10.5194/acp-23-10901-2023

[28] Kellner, E., Baird, A.J., Oosterwoud, M., *et al.*: Effect of temperature and atmospheric pressure on methane (CH_4) ebullition from near-surface peats. Geophys. Res. Lett. **33**(18), L18405 (2006) https://doi.org/10.1029/2006GL027509

[29] Tokida, T., Miyazaki, T., Mizoguchi, M., *et al.*: Falling atmospheric pressure as a trigger for methane ebullition from peatland. Glob. Biogeochem. Cycles **21**(2), GB2003 (2007) https://doi.org/10.1029/2006GB002790

[30] Baird, A.J., Beckwith, C.W., Waldron, S., Waddington, J.M.: Ebullition of methane-containing gas bubbles from near-surface Sphagnum peat. Geophys. Res. Lett. **31**(21), L21505 (2004) https://doi.org/10.1029/2004GL021157

[31] Glagolev, M.V., Kleptsova, I.E.: Mechanism of methane bubble transport from peat layer (in Russian). Environ. Dyn. Glob. Clim. Change **3**(3), 54–63 (2012) https://doi.org/10.17816/edgcc3354-63

[32] Cole, J.J., Caraco, N.F.: Atmospheric exchange of carbon dioxide in a low-wind oligotrophic lake measured by the addition of SF_6. Limnol. Oceanogr. **43**(4), 647–656 (1998) https://doi.org/10.4319/lo.1998.43.4.0647

[33] Wanninkhof, R.: Relationship between wind speed and gas exchange over the ocean. J. Geophys. Res. Oceans **97**(C5), 7373–7382 (1992) https://doi.org/10.1029/92JC00188

[34] Lions, J.-L.: Quelques Méthodes de Résolution des Problèmes aux Limites Non Linéaires. Dunod, Gauthier-Villars, Paris (1969)

[35] Ladyzhenskaya, O.A., Solonnikov, V.A., Ural'tseva, N.N.: Linear and Quasi-linear Equations of Parabolic Type. Translations of Mathematical Monographs, vol. 23. American Mathematical Society, Providence (1968)

[36] Evans, L.C.: Partial Differential Equations, 2nd edn. Graduate Studies in Mathematics, vol. 19. American Mathematical Society, Providence (2010). https://doi.org/10.1090/gsm/019

[37] Il'in, A.M.: Differencing scheme for a differential equation with a small parameter affecting the highest derivative. Math. Notes Acad. Sci. USSR **6**(2), 596–602 (1969) https://doi.org/10.1007/BF01093706

[38] Scharfetter, D.L., Gummel, H.K.: Large-signal analysis of a silicon Read diode oscillator. IEEE Trans. Electron Devices **16**(1), 64–77 (1969) https://doi.org/10.1109/T-ED.1969.16566

[39] Samarskii, A.A.: The Theory of Difference Schemes. Marcel Dekker, New York (2001)

[40] Oberkampf, W.L., Roy, C.J.: Verification and Validation in Scientific Computing. Cambridge University Press, Cambridge (2010). https://doi.org/10.1017/CBO9780511760396